Graphene oxide and graphene nanosheet reinforced aluminium matrix composites: Powder synthesis and prepared composite characteristics

Jinghang Liu, Umar Khan, Jonathan Coleman, Bea Fernandez, Pablo Rodriguez, Sumsun Naher, Dermot Brabazon

PII: S0264-1275(16)30032-6
DOI: doi: 10.1016/j.matdes.2016.01.031
Reference: JMADE 1232

To appear in:

Received date: 4 November 2015
Revised date: 5 January 2016
Accepted date: 7 January 2016

Please cite this article as: Jinghang Liu, Umar Khan, Jonathan Coleman, Bea Fernandez, Pablo Rodriguez, Sumsun Naher, Dermot Brabazon, Graphene oxide and graphene nanosheet reinforced aluminium matrix composites: Powder synthesis and prepared composite characteristics, (2016), doi: 10.1016/j.matdes.2016.01.031

Graphene Oxide and Graphene Nanosheet Reinforced Aluminium Matrix Composites: powder synthesis and prepared composite characteristics

Jinghang Liu [1,2], Umar Khan [3], Jonathan Coleman [3], Bea Fernandez [1,2], Pablo Rodriguez [1,2], Sumsun Naher [1,4], and Dermot Brabazon [1,2,a]

[1] Advanced Processing Technology Research Centre, Dublin City University, Dublin 9, Ireland

[2]School of Mechanical & Manufacturing Engineering, Dublin City University, Dublin 9, Ireland

[3]School of Physics, Trinity College Dublin, Dublin 2, Ireland

[4]Department of Mechanical Engineering and Aeronautics, City University London, UK

[a]dermot.brabazon@dcu.ie

Keywords: aluminium matrix composites (AMCs), graphene nanosheets (GNSs), graphene oxide (GO), powder metallurgy (P/M), compaction, sintering.

Abstract. The preparation and properties of reduced graphene oxide (rGO) and graphene nanosheets (GNSs) reinforcement of aluminium matrix nanocomposites (AMCs) are reported. For the rGO-AMCs, commercial colloidal GO was coated onto aluminium powder particles and then reduced via thermal annealing. For the GNS-AMCs, graphene exfoliated from graphite through ultrasonication and centrifugation was coated onto aluminium particle surfaces via dispersion mixing, filtering and drying. Pure aluminium and aluminium composites with various reinforcement concentrations of rGO and GNS were cold compacted into disc-shaped specimens and sintered in inert atmosphere. The mechanical properties and microstructure were studied and characterised via Vickers hardness, X-ray diffraction, density measurement, and scanning electron microscopy. The reinforcements were uniformly distributed onto the aluminium particle surfaces before and after consolidation within the composites. The relevant factors for the powder metallurgy process (compaction pressure, density, and sintering conditions) were optimised. Increased levels of increased hardness were recorded, over baseline compacted and sintered pure aluminium samples, prepared under identical experimental conditions, of 32% and 43% respectively for the 0.3wt.% rGO-Al and 0.15wt.% GNSs-Al composites. The process developed and presented herein provides encouraging results for realising rGO-AMC and GNS–AMC nanocomposites via low cost cold powder compaction and sintering metallurgy techniques.

1. Introduction

Aluminium matrix composites (AMCs) have been widely studied since the 1920s. In the last few years AMCs have been utilized in both high-tech structural and functional applications including aerospace, defense, automotive, thermal management, sports and recreation, electronic packaging, and armour [1]. These composites are utilised as substitutes for monolithic materials including aluminium, ferrous, titanium alloys and polymer based composites. Alumina and silicon carbide reinforcements are commonly utilised in AMCs. The tensile strength of alumna and SiC being on the order of 300 MPa is much below that of graphene at 130 GPa. A small percentage of GNS or even rGO could therefore increase the overall composite physical properties greatly. The electrical conductivity of graphene is similarly an order of magnitude greater than that of aluminium. With such increased strength and conductivity, power transmission lines would therefore be a good end application for AMCs developed based on these reinforcements. Several papers have recently been published on carbonaceous-reinforced aluminium composites e.g., single or multi-walled carbon nanotubes SWNTs/MWCNTs [2-11]. To achieve the integration of CNTs into AMCs, the following methods have been used: mechanical dispersing, e.g., ball milling process [3], friction stir process [8-10], solvent dispersion e.g., ethanol with surfactant/ultrasonic support [12], or hybrid methods of the above [13]. It has been reported that the large aspect ratio of CNTs (wt.%>2) was difficult to

disperse and thus the potential of higher improvements in mechanical properties of CNTs-Al composites are relatively limited [3]. Undesirable reactions between CNTs and the aluminium matrix, e.g., carbide formation, have also been observed in certain CNTs-Al composites [6, 14]. It has further been inferred experimentally that many voids have been formed based on the provision of nucleation sites on CNTs, which would eventually lead to premature fracture of AMCs specimens during loading application [11]. The following factors are considered as challenging in the applications of CNTs in Metal Matrix Composites (MMCs): non-standardized raw CNTs materials, high remaining porosities, and introduction of longitudinal alignment after certain manufacture procedures (e.g. extrusion) and complex interface design [15].

As alternatives to conventional AMCs reinforcements, e.g., equiaxed ceramic, short fibres, whiskers, continuous fibres, and monofilament [1], graphene and its derivative reinforcements are attracting increasing attention since single layers of graphene were first produced in 2004 [16]. Compared with CNTs, graphene oxide provides many conveniences and advantages for use as reinforcement in AMCs, for instant, graphene oxide is water-soluble due to the presence of hydrophilic groups (e.g., carboxyl, carbonyl, and hydroxyl) so that it is easier to handle and to disperse in water or other organic solvents as well as in different matrixes, so that agglomeration of the porosities can be significantly reduced or fully avoided. Meanwhile, graphene oxide can be synthesised in large quantities from inexpensive graphite powder and solubilised in a variety of solvents [17, 18]. When using graphene oxide, the reduction process is necessary to remove the oxygen groups from the structure of the graphene oxide sheets. Reducing graphene oxide nanosheets to rGO will partly restore the structure and properties of graphene. This mechanism can be done by thermal annealing reduction, chemical reduction or multi-step reduction [19]. To exclude or consume the residual oxygen in the atmosphere, vacuum, inert atmosphere or reducing atmosphere is normally used during annealing reduction. In previously published work GO has been thermally reduced to rGO by heating at 500°C for 2h in Ar/H_2 (5 vol.% H_2) 40 ml/min [20], at 450°C for 2h in an Ar/H_2 (1:1), 100 ml/min [21], and under the condition of 550°C for 2h in pure Ar [22]. It has been reported that the oxygen-containing groups in GO can also be efficiently removed in a hydrogen atmosphere at 100-200°C [23].

A lot of research work has been conducted on the fabrication of aluminium composites based on reinforcing with graphene nanosheets [14, 24, 25], graphene nanoflakes (GNFs) [24, 26, 27], few-layered graphene (FLG) [28], or its derivatives graphene oxide and reduced graphene oxide [20, 22]. Reported input control factors for the nano-reinforced matrix composite synthesis are listed in Table 1. Cold compaction followed by hot isostatic pressing (HIP) [24], as well as hot extrusion [14, 22, 26, 27], vacuum hot press and/or hot rolling [28] are commonly used in the literature to manufacture the solid pure aluminium and reinforced rGO-AMCs and GNS-AMCs specimens. The same processes are also found for CNTs-Al composites [6]. Using conventional powder metallurgy compaction and sintering could be a replacement for these more expensive hot extrusion, vacuum hot pressing, and hot rolling processes. If this was achievable, this could allow for conventional powder metallurgy processes to be more widely used by industry for nano-reinforced metal matrix composite mass scale production. It is know that aluminium alloy powders can provide full density at sufficiently high compaction pressure [29]. In other work, unalloyed aluminium powders (<20μm) were also found consolidated to 100% density under the pressure of 1 GPa [30]. A wide range of compaction pressures have been reported, typically ranging from 50 to 600 MPa, for the production of SWNTs/MWCNTs-AMCs [2-4, 6, 7, 11] and graphene and its derivatives based AMCs [20, 22, 27, 31-33].

While fabricating AMC with rGO and GNSs as reinforcements, the following target process aims should be set: 1) to uniformly distribute reinforcement within the AMCs; 2) to effectively reduce the GO nanosheets to rGO and avoid introducing deformations, e.g., wrinkling and folding of the rGO

and graphene sheets; and 3) to achieve a strong bonding between nanosheets and aluminium particles. The production of rGO and GNS reinforced AMCs via the powder metallurgy route is examined in this paper with a view to taking advantage of these reinforcement materials for provision of improved AMC properties.

Material	Compaction	Sintering	Specific details
Atomized Al average size ~22 μm; 0.1 wt.% GNSs (-18% TS), and 1.0 wt.% MWNT (+12% TS) [14]	instrumented hot isostatic pressing (I-HIP): ~375°C, ~20 mins	NA	ϕ ~20mm billets: preheated to ~550°C, 4 h; extrusion: 50 tons, 4:1 ratio, ~12.5mm/s, ~65ksi (448kPa)
Ball-milled Al flakes 2μm thick; 0.3 wt.% GO (+62%TS) [22]	ϕ 40×30mm billets	sintering: 580ºC, Ar., 2h	hot extrusion: 440ºC, 20:1 ratio
As received Al 1-3μm (99%) ; 0.3wt.% GNPs (+11.1%UTS, +14.7% YS) [27]	ϕ30x30mm billets: 170MPa	muffle furnace: 600ºC, 6h	ϕ9/16mm rods: hot extrusion,470ºC, 1m/min
Ball milled Al flakes from particle size ϕ10 μm; 0.3wt.% rGO (+18% elastic modulus, +17% hardness) [20]	billet compaction: 500MPa	vacuum hot press: 530 ºC, 600MPa, 1h	NA
Ball milled Al 45 μm (99.5%) ; SiC:GNSs(17wt.%) (+45%TS, +84% tensile ductility) [25]	NA	powder injection into A356 Al alloy, cooled to 605ºC	stirred at 400rpm for 5 min, adding 1 wt.% Mg
Gas-atomized spherical Al gain size ~15-20 μm (99.5%); 0.5 wt.% GNFs (+8.8%YS, +17.7%UTS) [26]	NA	NA	ϕ15mm bar: extruded at 300ºC followed by annealing at 300ºC, 2h
Al particle < ϕ150μm (99.5%); 0.7 vol.% FLG (+71.8%TS) [28]	compacted in copper tube: ϕ60mm ×150mm high ×1.5mm thick	NA	hot rolling: 500ºC, 15ºC /min, 12% reduction per pass
Gas-atomized Al-Mg (1.5wt.%)-Cu (3.9wt.%) powder; 0.3wt.% GNFs (+25% TS, +58%YS) [24]	preheat in tube: 300-400 ºC, 2h, 1×10^{-2}Pa, cooled to room temp.;	NA	HIP: 480ºC, 150MPa, 2h; hot pressing: 400-480ºC, 10:1 ratio, 3mm/min, 300kN; 495ºC/30min, +96h

Table 1: Reported compaction and sintering input factors for AMC nanocomposites fabrication.

2. Experimental procedure

Aluminium powder 250 mesh (purity >99.5 %) was purchased from East Coast Fibreglass Ltd (South Shields, UK). The morphology of synthesised GNSs-Al powder is shown in Figure 1 (a) and the particle size distribution of the as-received aluminium powder is shown in Figure 1 (b). The SEM

images were recorded with an Evo LS15, Carl Zeiss SEM. Disc specimens were fabricated via the powder metallurgy route with the different weight percent of nanoparticle reinforcements as listed in **Table 2**.

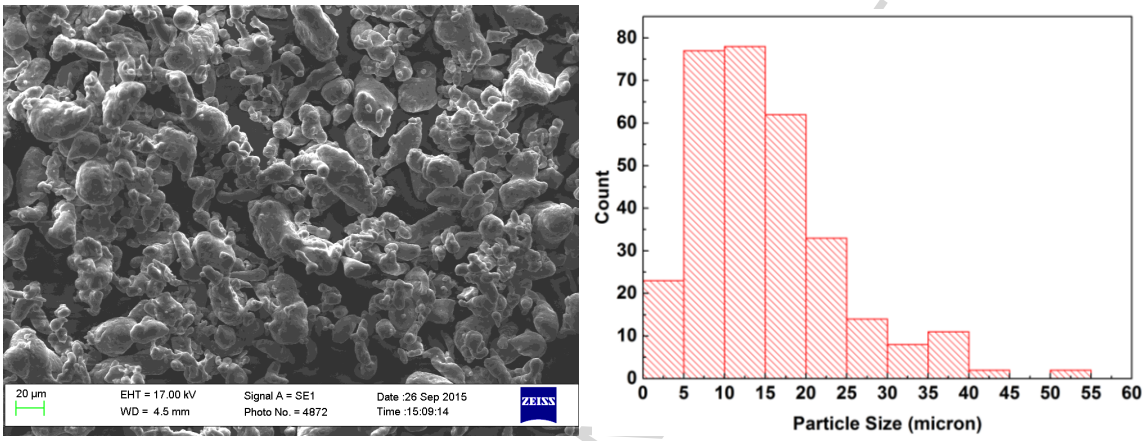

(a) (b)

Figure 1: (a) SEM image of particle morphology of synthesised GNSs-Al and (b) particle size distribution of as-received aluminium powder.

Material	Source	Weight percent of reinforcements
GNSs-AMCs	synthesised	0.07wt.%, 0.1wt.%, and 0.15 wt.%
rGO-AMCs	synthesised	0.07wt.%, 0.15wt.%, 0.3wt.%, 0.7wt.%, and 2wt.%

Table 2: Compositions prepared of rGO-AMC and GNSs-AMC powders.

Water based graphene oxide colloid (4mg/ml, monolayer >95%) was purchased from Graphenea (Gipuzkoa, Spain). The rGO-Al powder the aluminium powder was firstly scaled and mechanically stirred with various solvents using concentration of 200 ml per 5g Al, for 15 mins. In order select the best solvent for this process step, acetone (>99%), ethanol (>99%), and ethanol-water (80-20%) were trialed. The graphene oxide water colloid was sonicated for one to three hours, depending on the weight percent applied, in order to uniformly disperse the graphene oxide particles. Afterwards the sonicated dispersion was added slowly drop by drop to the aluminium slurry obtained from the previous steps. Mechanical stirring was then started and continued until the dispersion tubribty became uniform. Filtering of the as-synthesised powder dispersion, from the liquid solvents, was performed through 11 micrometer Whatman filter paper. The filtered powder was then dried and thermally reduced in a horizontal tube furnace at 550ºC for 2h in an argon atmosphere with a gas flow rate of 30ml/min. With other parameters being the same, the most clear solutions after mechanical stirring occurred in the order of acetone > ethanol-water > ethanol (see Figure 2). Acetone was therefore selected as the solvent of choice for further testing. A stirring time of 1h was sufficient to obtain fully clear dispersions for the 0.07, 0.15, and 0.3 wt.% GO-Al dispersion in acetone, while in comparison, 3h and 5h were required respectively for 0.7 and 2 wt.% GO-Al powders. The brown colour remaining on the filter papers used for the 0.7wt.% and 2 wt.% GO-Al powders indicates the large amount of remaining graphene oxide particles in the solvent for these compositions (see Figure 3) which were not bonded to the aluminium particles. For this reason, only the rGO-AMCs powders of 0.07wt.%, 0.15wt.%, and 0.3wt.% were processed via the powder metallurgy route for composite synthesis.

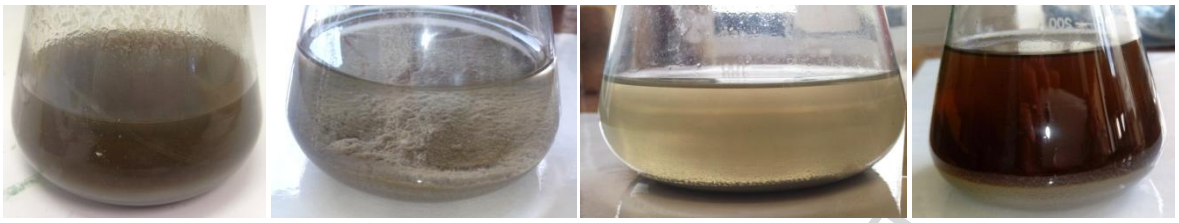

(a) (b) (c) (d)

Figure 2: Visual characteristics observation is a direct way to see the effect of solvent and stirring time: 2wt.% GO-Al dispersion with stirring time of (a) 1 h in acetone, (b) 5h in acetone, (c) 5h in ethanol-water, and (d) 5h in ethanol.

(a) (b) (c) (d) (e)

Figure 3: GO-Al powder filtered from acetone with stirring time and concentrations of (a) 1h, 0.07wt.%, (b) 1 h, 0.15wt.%, (c) 1 h, 0.3wt.%, (d) 3 h, 0.7wt.%, and (e) 5 h, 2wt.%.

To prepare GNSs-Al powder, Etyle cellulose (EC) was dissolved in Isopropyl alcohol (IPA) at a concentration of 15mg/ml. Graphite was added to the EC/IPA solution (100mg/ml) and exfoliated by ultrasonication under sonic probe for 72 h. Centrifugation was carried out to separate unexfoliated graphite from exfoliated graphene (Gr). Graphene was centrifuged at 500 rpm for 45 mins, the top 80% of the supernatant was collected. To remove/washout dissolved EC from graphene, the supernatant was centrifuged at 2000 rpm for 3h. Clear supernatant was discarded and graphene sediment was kept. This step was repeated four times. An IPA/EC (2mg/ml) solution was prepared. The washed graphene was added to this solution and concentration was measured by filtration of know volume of Gr dispersion through a filter membrane of known mass. This dispersion was used as stock graphene dispersion. As-received aluminium powder was also dispersed in EC/IPA solution. Required volumes of graphene were added (from the stock dispersion) to Al/EC/IPA dispersions to make various mass fraction Gr/Al/EC/IPA composite dispersions. Each dispersion was mixed for 48h by magnetic stirring and then filtered through a PET filter membrane (pore size 0.45 microns). The residue was dried in an oven for another 48h at 60 ºC.

In this paper, the as-received and synthesised powders were cold compacted at the pressures of 30, 73, 220, 260, 330, and 560 MPa to investigate their compaction behaviours. Sample powder weights of 0.75 g were cold compacted in evacuable pellet dies of 20 mm diameter within an automatic uniaxial hydraulic press (Atlas 40T press, Specac Limited, Kent, UK). The thickness of the resulting green specimen was 1 mm. A thin layer of rhombic boron nitride powder was physically coated onto the die surfaces as an aid to sample removal.

Before sintering, the solidus and liquidus temperatures of the powders used were firstly determined using differential thermal analysis (DTA) shown in

Figure 4. In this study, the effects of sintering conditions, e.g., atmosphere, temperatures, holding time and heating rate, were investigated and optimized. The horizontal tube furnace (Carbolite 3216 with Eurotherm controller) was used with the optimized sintering conditions of 5°C/min from room temperature to 600°C (~ 88% of the melting temperature of the pure aluminium power), with a holding period of 4h and in an argon atmosphere.

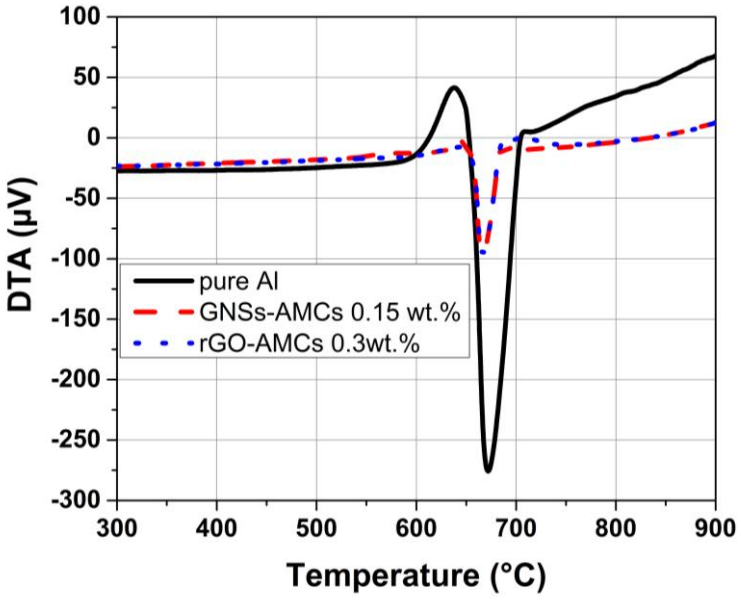

Figure 4: DTA values vs. temperature; maximum temperature set to 900 °C, ramp rate set to 10 °C/min, measurement interval at 1 s, and atmosphere was N_2 with a flow rate of 30ml/min for ~32 mg of aluminium, rGO-AMCs 0.3 wt.%, and GNSs-AMCs 0.15wt.% powder samples.

Results and Discussion

The morphologies of the pure aluminium and prepared composite powders are shown in Figure 5. The pristine aluminium particles appear smooth and with uniform colour intensity whereas the rGO and GNS on the aluminium particle surfaces are indicated by the surface shading.

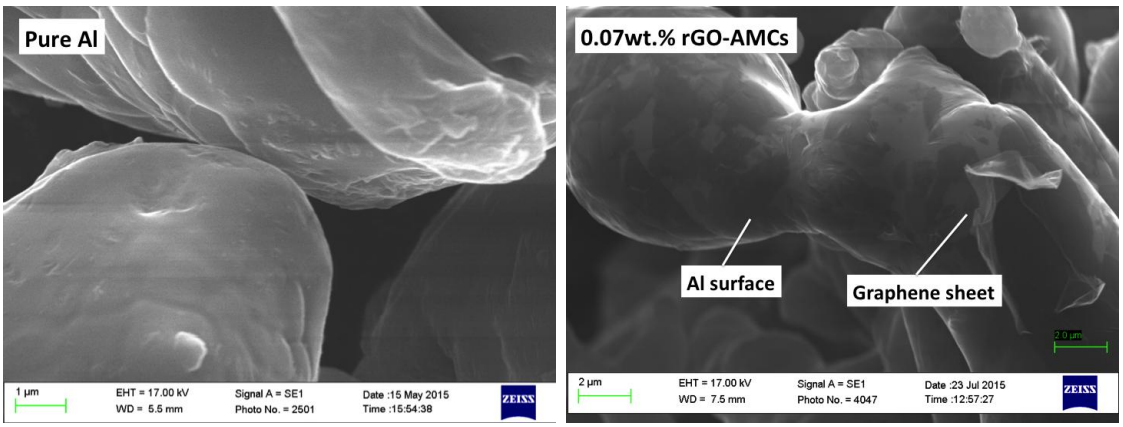

(a) (b)

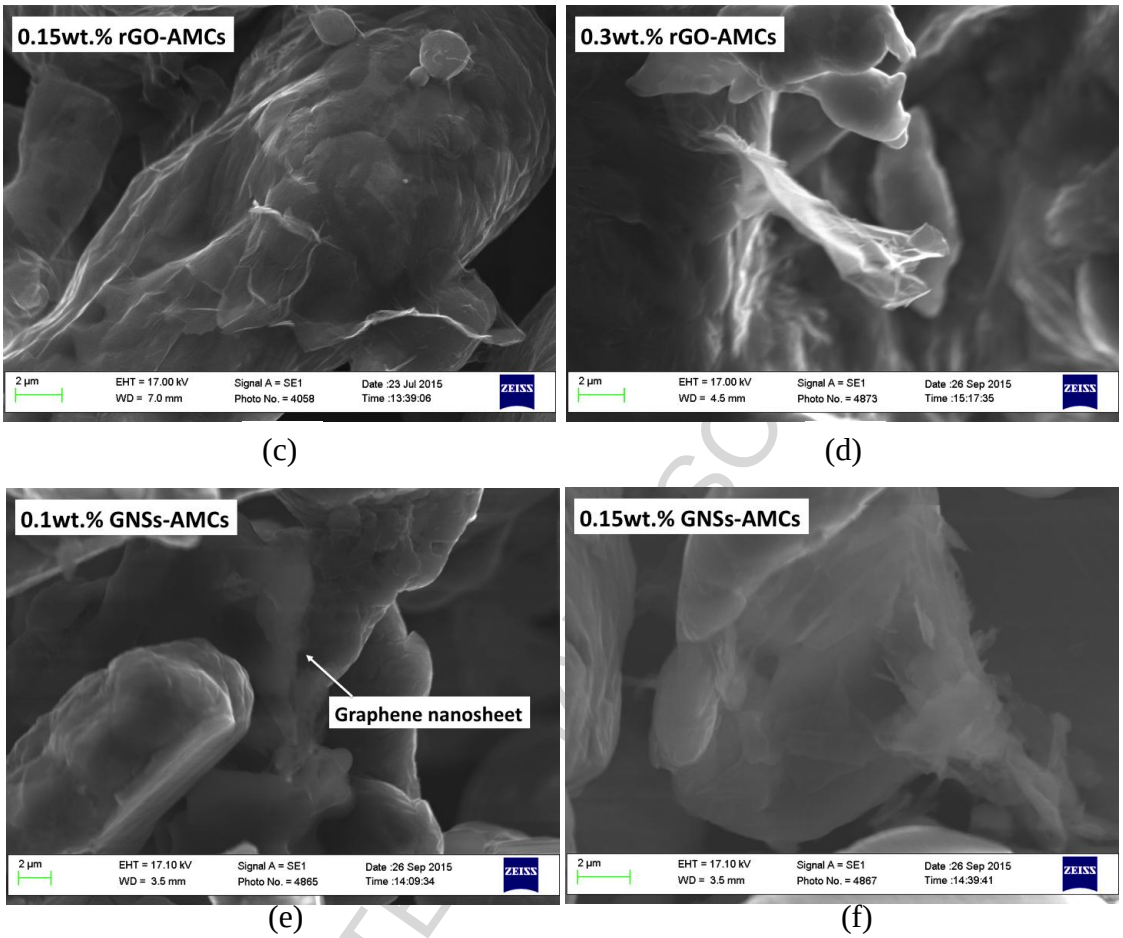

Figure 5: SEM photos of particle surface morphology of the powder particles of (a) pure aluminium, (b) 0.07 wt.% rGO-AMCs, (c) 0.15 wt.% rGO-AMCs, (d) 0.3 wt.% rGO-AMCs, (e) 0.1 wt.% GNSs-AMCs, and (f) 0.15wt.% GNSs-AMCs.

The theoretical solid density of aluminium is 2.699 g/cm^3. The densities of the green and the sintered samples were measured by the Archimedes method, the results of which are summarised in Figure 6. For higher the applied pressures, higher green densities were recorded as would be expected. For the pressure levels used in this study, completely pore free sample densities were not achieved. The density obtained at the maximum pressure of 560 MPa was 88.5% of the theoretical pore-free density.

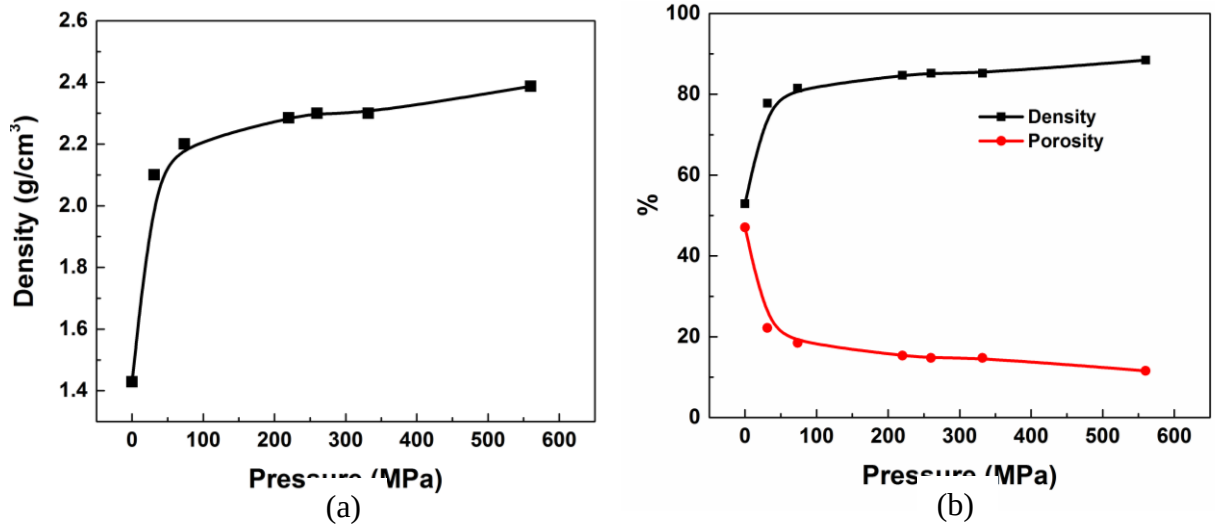

Figure 6: (a) Pressure vs. green density of pure aluminium specimens, and (b) percentage sintered density as functions of cold compacting pressure for aluminium samples.

The mixture density, δ_m, was calculated by the rule of mixtures, using the theoretical density 2.699 g/cm^3 for pure aluminium powder and approximately 2.0 g/cm^3 for both rGO and GNS, as follows.

$$\delta_m = \frac{100}{\frac{w_{al}}{\rho_{al}} + \frac{w_g}{\rho_g}} \quad \textbf{(1)}$$

ρ_{al} - specific weight of the base aluminium powder;

w_{al} - weight percentage of the aluminium powder;

ρ_g - specific weight of graphene films, approximately 2.0 g/cm^3;

w_g - weight percentages of additive, graphene sheets.

Based on equation (1), the densities of the nano-reinforced AMCs were expected to be decreased by less than 1% compared with the density of pure aluminum powder. The theoretically achievable and measured densities of AMCs are presented in Figure 7.

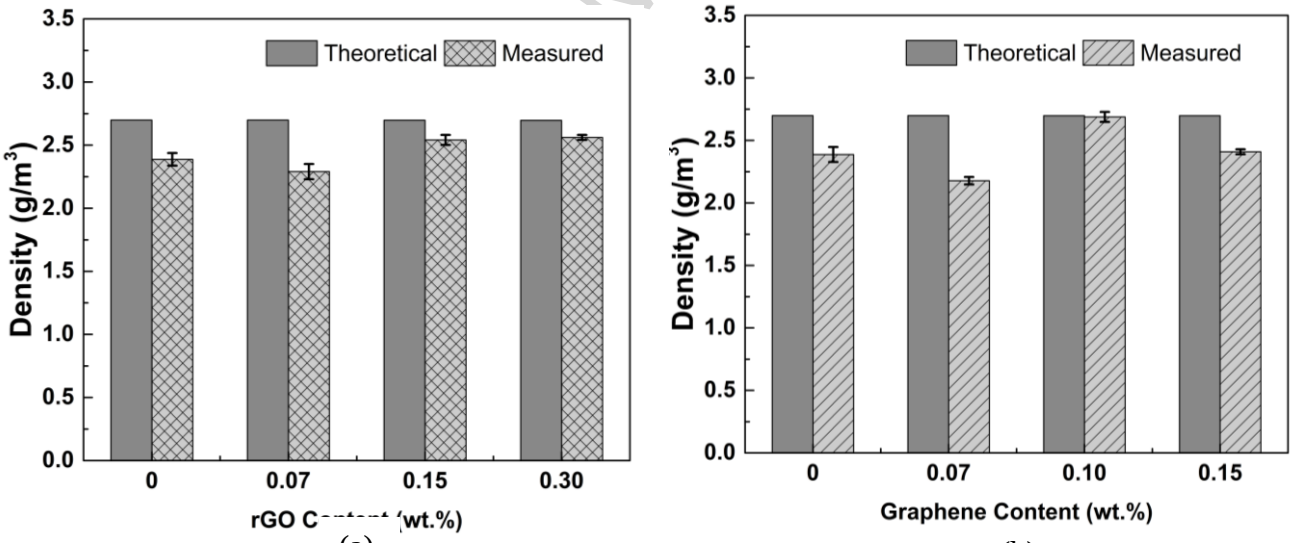

Figure 7: Density vs. weight percentage of (a) rGO and (b) GNS for the AMC samples compacted at 560 MPa.

Vickers hardness values were measured with a Leitz micro hardness tester (Semiconductor GmbH, Wetzlar, Germany) with a 981mg loaded weight. The measurements were repeated six times for each sample at random surface locations and averaged. The hardness results from the pure aluminium, the rGO and GNSs reinforced aluminium matrix composites samples are summarized in Figure8. The hardness of the base material, pure aluminium sample, was 26.0±1.3HV, while the hardness of 0.3wt.% rGO-AMCs and 0.15 wt.% GNSs-AMCs samples were 34.5±3.0 and 37.6±2.3HV respectively, showing 32% and 43% increments over the unreinforced aluminium under otherwise identical experimental sample compaction and sintering conditions.

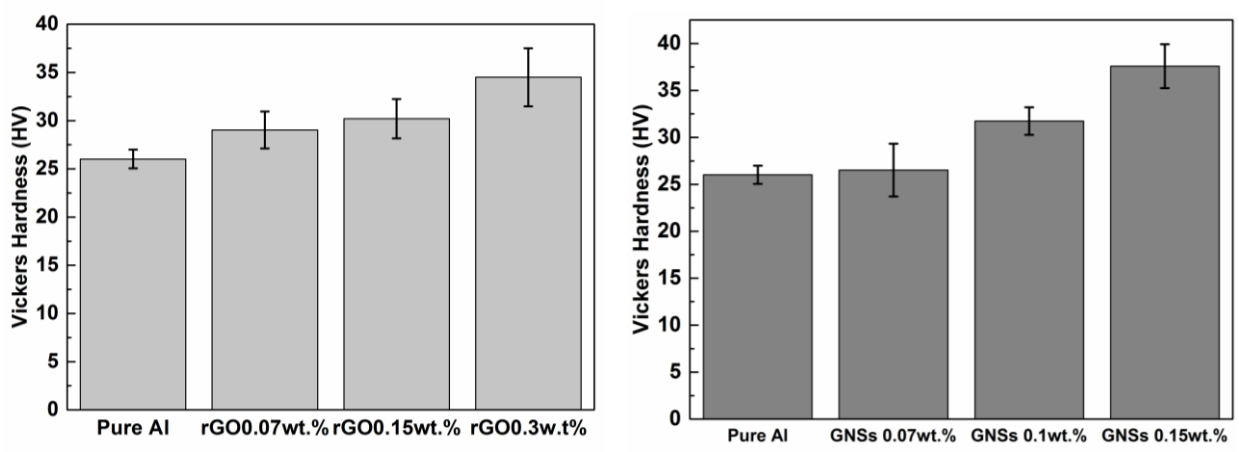

(a) (b)

Figure 8: The Vickers hardness of the pure aluminium, rGO-AMCs, and GNSs-AMCs specimens.

Material	wt.%	Vickers hardness HV	Increment over pure Al
Pure Al	NA	26.0±1.3	NA
rGO-AMCs	0.07	29.0±1.9	11%
	0.15	30.2±2.0	16%
	0.3	34.5±3.0	32%
GNSs-AMCs	0.07	26.5±2.8	1.9%
	0.1	31.7±1.4	21%
	0.15	37.6±2.3	43%

Table 3: The Vickers hardness values and the percentage increase, over that of the pure aluminium sample, of the rGO-AMCs and GNSs-AMCs samples, n=6.

Representative XRD scans for the pure aluminium, GNSs and rGO-AMC nanocomposites are presented in Figure 9. All samples have major aluminum peaks at 38.8° (1 1 1), 45.0° (2 0 0), 65.4° (2 2 0), 78.5° (3 1 1) and 82.7° (2 2 2). Peaks for aluminium oxide (Al_2O_3) are observed at 27.1° in all samples. However, no aluminium carbide peak was recorded for any of the samples. The pure and nano-reinforced aluminium matrix composite samples were broken open by pressing a rounded 5 mm pin through the sample centre in order to examine their internal structure via SEM. The fracture surfaces of the pure aluminium and composites samples are shown in Figure 10. For all samples, the degree of sample compaction was higher at the sample surface compared to the sample centre. For the pure aluminium samples, the central section showed higher density compared with the GNSs and rGO reinforced samples. For the tested pressure levels, up to 560MPa, pores were still evident between the larger powder particles for the rGO-AMC and GNS-AMC samples.

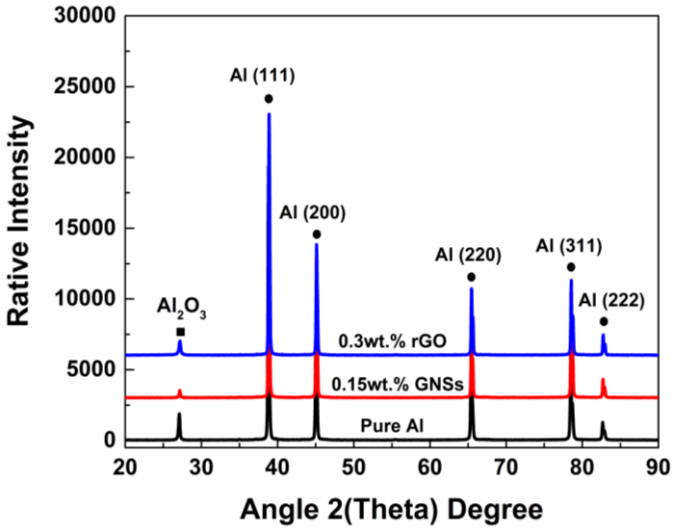

Figure 9: XRD scans of pure aluminium, 0.15wt.% GNSs-AMCs and 0.3wt.% rGO-AMCs PM samples.

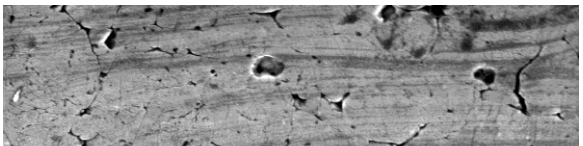

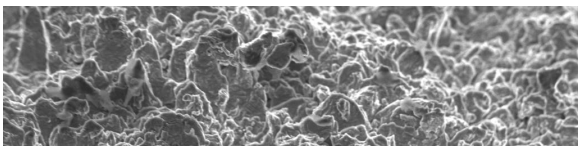

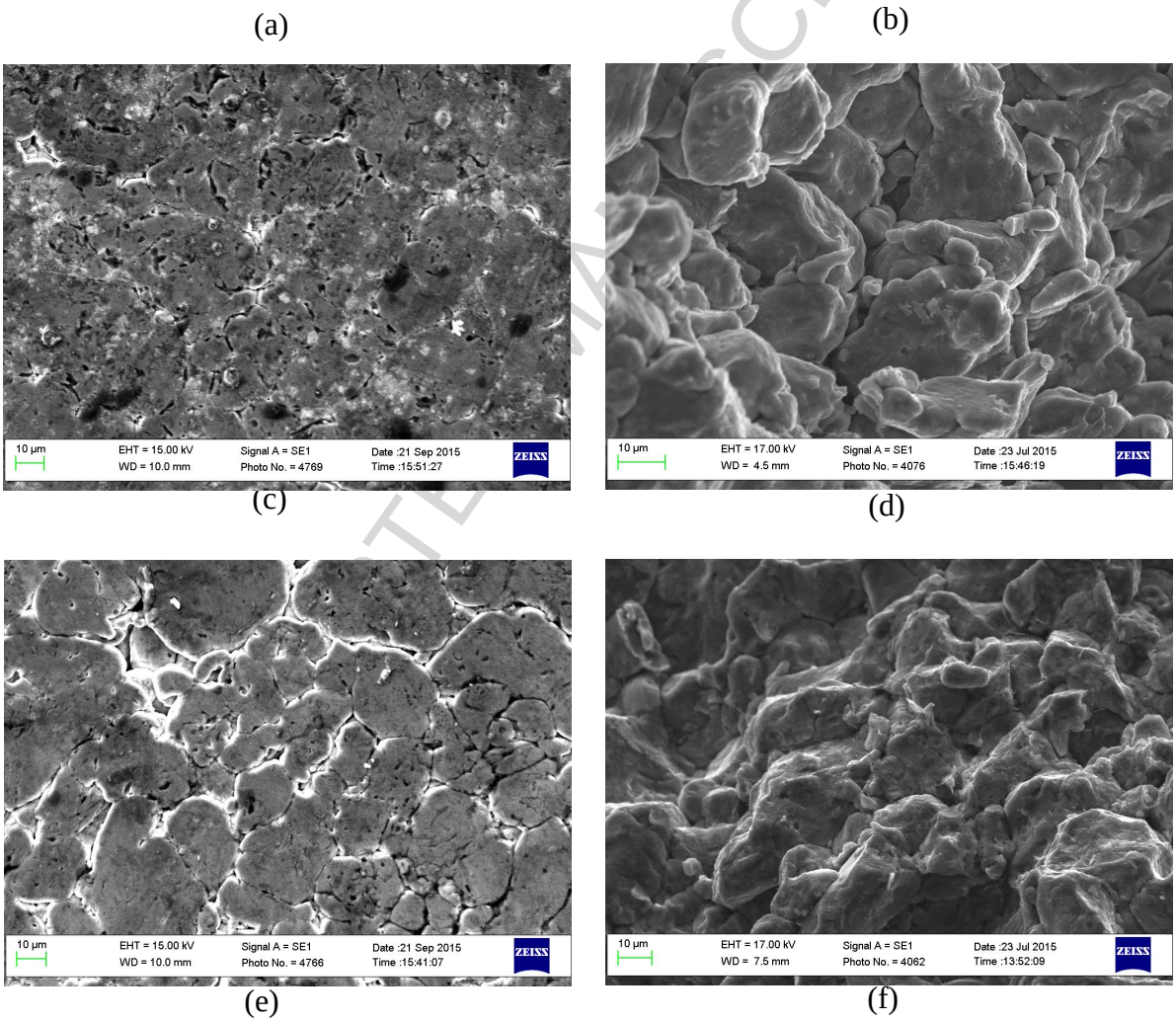

Figure 10: SEM photos of (a) top surface and (b) fractured internal structure of pure aluminium; (c) top surface and (d) fracture surface of rGO 0.3wt.% reinforced sample; (e) top surface and (f) fracture internal structure of GNSs 0.1wt.% reinforced sample.

Conclusion

In this paper, the effects of rGO and GNS content on the properties of the formed aluminium composites were investigated. The pure aluminium, rGO-AMCs, and GNSs-AMCs powders were cold compacted and sintered into consolidated disc specimens.

Two key factors need to be considered during the compaction process: the achieved radial and axial pressure distributions, as depicted in Figure 11. The radial pressure upon the inner surface of rigid cylindrical die wall is always smaller than the nominal axial pressure exerted by the piston of a hydraulic press due to the powder bulk being in solid form with no hydraulic properties.

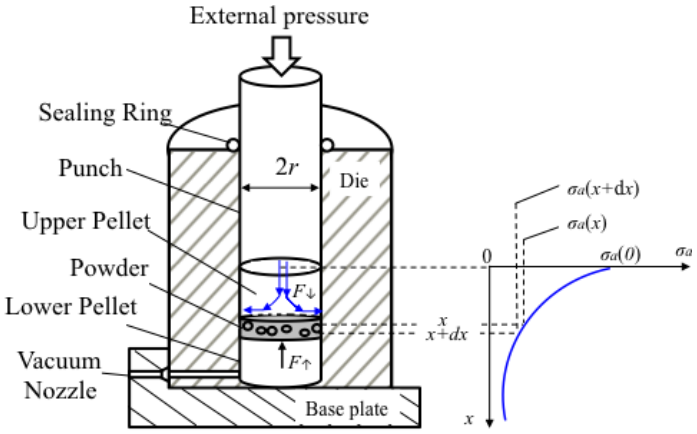

Figure 11: Powder compaction configuration and the axial stress distribution among the compacted disc sample, after [34].

The powder column in the die cavity can be imagined as stacked thin layers. As the upper pellet enters the die and compacts the powder, the initial axial stress is noted as $\sigma_a(0)$. Selecting one single layer at vertical distance x from the top compaction surface, and its height as dx, if the inner diameter of the compacting die is $2r$, then the cross-sectional area S_c and lateral area S_l of the selected layer would be as follows.

$$S_c = \pi r^2 \quad \textbf{(2)}$$

$$S_i = 2\,\pi r\,dx \quad \textbf{(3)}$$

The axial stress acting upon the bottom face of the layer is $\sigma_a(x+dx)$ which would be expected to be smaller than the axial stress acting upon the top face of the selected layer $\sigma_a(x)$ due to the presence of friction force exerting on the lateral face of the layer and the die wall. If the frictional force is assumed to be proportional to the axial stress and the lateral area of the layer, the equilibrium equations are then

$$F_{\downarrow} = \pi r^2\,\sigma_a(x) \quad \textbf{(4)}$$

$$F_{\uparrow} = \pi r^2\,\sigma_a(x+dx) \quad \textbf{(5)}$$

$$f = \mu\,2\,\pi r\,dx.\sigma_a(x) \quad \textbf{(6)}$$

where, $F_{\downarrow}$ represents the fore exerting on the top layer surface, $F_{\uparrow}$ represents the force acting upon the bottom face of the layer, μ is the friction coefficient and f represents the friction force exerted on the wall surface. From equation (4)-(6) it is noted that

$$d\sigma_a(x) = \sigma_a(x+dx) - \sigma_a(x) = -2\mu\,\sigma_a(x)dx / r \quad \textbf{(7)}$$

The integration of equation (7) provides the relationship between the top surface axial stress and the compaction distance as follows.

$$\sigma_a(x) = \sigma_a(0)\exp(-2\,\mu x/r) \quad \textbf{(8)}$$

The axial compressive stress available for the local densification of the powder $\sigma_a(x)$ decreases exponentially with increasing distance from the top surface. Assuming the process as a quasistatic process, that the friction coefficient μ is equal to 0.12 (steel-steel with lubricant), and that the stress on the top and bottom surfaces of the compacted sample equals to the nominal pressure applied, 560 MPa, then the stress at the middle natural area of sample is at the lower value of 528 MPa, a pressure which is 6% lower. From equation (8), therefore the stresses at each surface ends should be larger than in the midsection, which was found to result in zone of lower compaction density in the central disc regions.

During cold compaction, the higher the pressure resulted in a higher green density as expected. The density obtained at the maximum pressure of 560 MPa was 88.5% of the pore free density. However, significant hardness improvements measured for the GNSs and rGO-AMC composites are very encouraging results that this method could be developed for mass production of components. Apart from these promising results, the enhancement in the strength and conductivity of these composites requires further examination and development to actualize the potential of this new material. The possibility of using SiC nanoparticles wrapped by graphene sheets as carrier agents for the incorporation of these structures into AMCs is a promising new route [35] to achieve this.

The reduced graphene oxide and graphene nanosheets composites produced have shown improved mechanical reinforcements despite increased levels of porosity over the pure aluminium disk samples. The GNS reinforcement provided significantly higher increases in hardness for the same quantity of reinforcement, see Table 3. From this result, it could be concluded that being closer to the GNS provide enhanced reinforcement compared to the rGO reinforcement. The graphene nanoparticle reinforced aluminium composites could extend the use of aluminium materials, offering higher strength to weight ratios for typical AMC applications. In spite of the observed overall reinforcing effect, challenges for using these unique nanomaterials as reinforcement in AMCs still exist which require further research. To achieve maximum improvements, 1) effective and uniform dispersion, especially for rGO composites >0.7 wt.% should be sought to achieve greater mechanical properties; 2) unwrinkled graphene sheets in larger sizes would be preferred on the metal powder particles; 3) undesirable oxide formation on the aluminium matrix during powder metallurgy should be avoided (ball milling in protective liquids may be a technique to reduce or overcome this problem in future work); and 4) higher cold compaction pressures especially toward the central part of green samples would most likely be beneficial.

References

[1] M. K. Surappa, "Aluminium matrix composites: Challenges and opportunities," *Sadhana*, vol. 28, February/April 2003, pp. 319-334.

[2] H. Kwon, M. Estili, K. Takagi, T. Miyazaki, and A. Kawasaki, "Combination of hot extrusion and spark plasma sintering for producing carbon nanotube reinforced aluminum matrix composites," *Carbon*, vol. 47, 2009, pp. 570-577.

[3] A.M.K. Esawi, K. Morsi, A. Sayed, M. Taher, and S. Lanka, "Effect of carbon nanotube (CNT) content on the mechanical properties of CNT-reinforced aluminium composites," *Composites Science and Technology*, vol. 70, 2010, pp. 2237-2241.

[4] S. Singhal, R. Pasricha, S. Teotia, G. Kumar, and R. Mathur, "Fabrication and characterization of Al-matrix composites reinforced with amino-functionalized carbon nanotubes," *Composites Science and Technology*, vol. 72, 2011, pp. 103-111.

[5] H. Kwon, D. H. Park, J. F. Silvain, and A. Kawasaki, "Investigation of carbon nanotube reinforced aluminum matrix composite materials," *Composites Science and Technology*, vol. 70, 2010, pp. 546-550.

[6] A. M. K. Esawi, K. Morsi, A. Sayed, M. Taher, and S. Lanka, "The influence of carbon nanotube (CNT) morphology and diameter on the processing and properties of CNT-reinforced aluminium composites," *Composites Part A: Applied Science and Manufacturing*, vol. 42, 2011, pp. 234-243.

[7] L. Jiang, Z. Li, G. Fan, L. Cao, and D. Zhang, "The use of flake powder metallurgy to produce carbon nanotube (CNT)/aluminum composites with a homogenous CNT distribution," *Carbon*, vol. 50, 2012, pp. 1993-1998.

[8] Z. Liu, B. Xiao, W. Wang, and Z. Ma, "Singly dispersed carbon nanotube/aluminum composites fabricated by powder metallurgy combined with friction stir processing," *Carbon*, vol. 50, 2012, pp. 1843-1852.

[9] H. Izadi and A. P. Gerlich, "Distribution and stability of carbon nanotubes during multi-pass friction stir processing of carbon nanotube/aluminum composites," *Carbon,* vol. 50, 2012, pp. 4744-4749.

[10] Q. Liu, L. Ke, F. Liu, C. Huang, and L. Xing, "Microstructure and mechanical property of multi-walled carbon nanotubes reinforced aluminum matrix composites fabricated by friction stir processing," *Materials & Design,* vol. 45, 2013, pp. 343-348.

[11] A.M.K. Esawi, K. Morsi, A. Sayed, A. A. Gawad, and P. Borah, "Fabrication and properties of dispersed carbon nanotube–aluminum composites," *Materials Science and Engineering: A,* vol. 508, 2009, pp. 167-173.

[12] M.T. Hassan, A. M. Esawi, and S. Metwalli, "Effect of carbon nanotube damage on the mechanical properties of aluminium–carbon nanotube composites," *Journal of Alloys and Compounds,* vol. 607, 2014, pp. 215-222.

[13] R. George, K. Kashyap, R. Rahul, and S. Yamdagni, "Strengthening in carbon nanotube/aluminium (CNT/Al) composites," *Scripta Materialia,* vol. 53, 2005, pp. 1159-1163.

[14] S.F. Bartolucci, J. Paras, M. A. Rafiee, J. Rafiee, S. Lee, D. Kapoor, *et al.*, "Graphene–aluminum nanocomposites," *Materials Science and Engineering: A,* vol. 528, 2011, pp. 7933-7937.

[15] E. Neubauer, M. Kitzmantel, M. Hulman, and P. Angerer, "Potential and challenges of metal-matrix-composites reinforced with carbon nanofibers and carbon nanotubes," *Composites Science and Technology,* vol. 70, 2010, pp. 2228-2236.

[16] K.S. Novoselov, A. K. Geim, S. Morozov, D. Jiang, Y. Zhang, S. Dubonos, *et al.*, "Electric field effect in atomically thin carbon films," *Science,* vol. 306, 2004, pp. 666-669.

[17] K.P. Loh, Q. Bao, P. K. Ang, and J. Yang, "The chemistry of graphene," *Journal of Materials Chemistry,* vol. 20, 2010, pp. 2277-2289.

[18] H. C. Schniepp, J.-L. Li, M. J. McAllister, H. Sai, M. Herrera-Alonso, D. H. Adamson, *et al.*, "Functionalized single graphene sheets derived from splitting graphite oxide," *The Journal of Physical Chemistry B,* vol. 110, 2006, pp. 8535-8539.

[19] S. Pei and H.-M. Cheng, "The reduction of graphene oxide," *Carbon,* vol. 50, 2012, pp. 3210-3228.

[20] Z. Li, G. Fan, Z. Tan, Q. Guo, D. Xiong, Y. Su, *et al.*, "Uniform dispersion of graphene oxide in aluminum powder by direct electrostatic adsorption for fabrication of graphene/aluminum composites," *Nanotechnology,* vol. 25, 2014, 325601, pp.1-8.

[21] Z.-S. Wu, W. Ren, L. Gao, B. Liu, C. Jiang, and H.-M. Cheng, "Synthesis of high-quality graphene with a pre-determined number of layers," *Carbon,* vol. 47, 2009, pp. 493-499.

[22] J. Wang, Z. Li, G. Fan, H. Pan, Z. Chen, and D. Zhang, "Reinforcement with graphene nanosheets in aluminum matrix composites," *Scripta Materialia,* vol. 66, 2012, pp. 594-597.

[23] D. Wan, C. Yang, T. Lin, Y. Tang, M. Zhou, Y. Zhong, *et al.*, "Low-Temperature Aluminum Reduction of Graphene Oxide, Electrical Properties, Surface Wettability, and Energy Storage Applications," *ACS Nano,* vol. 6, 2012, pp. 9068-9078.

[24] S.-j. Yan, Y. Cheng, H. Qi-hu, C. Jun-zhou, L. Da-bo, and D. Sheng-long, "Research of Graphene-reinforced Aluminum Matrix Nanocomposites," Journal of Materials Engineering, *4,* 2014, pp. 1-6.

[25] A. F. Boostani, S. Tahamtan, Z. Jiang, D. Wei, S. Yazdani, R. A. Khosroshahi, *et al.*, "Enhanced tensile properties of aluminium matrix composites reinforced with graphene encapsulated SiC nanoparticles," *Composites Part A: Applied Science and Manufacturing,* vol. 68, 2015, pp. 155-163.

[26] J. L. Li, Y. C. Xiong, X. D. Wang, S. J. Yan, C. Yang, W. W. He, *et al.*, "Microstructure and tensile properties of bulk nanostructured aluminum/graphene composites prepared via cryomilling," *Materials Science and Engineering: A,* vol. 626, 2015, pp. 400-405.

[27] M. Rashad, F. Pan, A. Tang, and M. Asif, "Effect of Graphene Nanoplatelets addition on mechanical properties of pure aluminum using a semi-powder method," *Progress in Natural Science: Materials International 24, 2*, 2014, pp. 101-108.

[28] S. E. Shin, H. J. Choi, J. H. Shin, and D. H. Bae, "Strengthening behavior of few-layered graphene/aluminum composites," *Carbon*, vol. 82, 2015, pp. 143-151.

[29] M. Djuricic, M. Dragojlovic, and R. Novakovic, "Cold Sintering of Aluminum and Its Alloys " *Science of Sintering*, vol. 18, 1986, pp. 87-89.

[30] G. E. Totten and D. S. MacKenzie, *Handbook of Aluminum: Vol. 1: Physical Metallurgy and Processes*: Taylor & Francis, 2003.

[31] A. Gökçe and F. Fındık, "Mechanical and physical properties of sintered aluminum powders," *Journal of Achievements in Materials and Manufacturing Engineering*, vol. 30, 2008, pp. 157-164.

[32] T. Pieczonka, T. Schubert, S. Baunack, and B. Kieback, "Sintering Behaviour of Aluminium in Different Atmospheres," in *4th International Conference on Science, Technology and Applications of Sintering, Grenoble, France*, 2005, pp. 331-334.

[33] C. He, N. Zhao, C. Shi, and S. Song, "Mechanical properties and microstructures of carbon nanotube-reinforced Al matrix composite fabricated by in situ chemical vapor deposition," *Journal of Alloys and Compounds*, vol. 487, 2009, pp. 258-262.

[34] G. Bockstiegel, "A Simple Formula for the Calculation of Spatial Size Distributions from Data Found by Lineal Analysis," in *Stereology*, H. Elias, Ed., ed: Springer Berlin Heidelberg, 1967, pp. 193-194.

[35] Boostani, A.F., Yazdani, S., Mousavian, R.T., Tahamtan, S., Khosroshahi, R.A., Weid, D., Brabazon, D., Xu, J.Z., Zhang, X.M., Jiang, Z.Y., Strengthening mechanisms of graphene sheets in aluminium matrix nanocomposites, Materials & Design, 88, 2015, pp. 983-989, doi:10.1016/j.matdes.2015.09.063

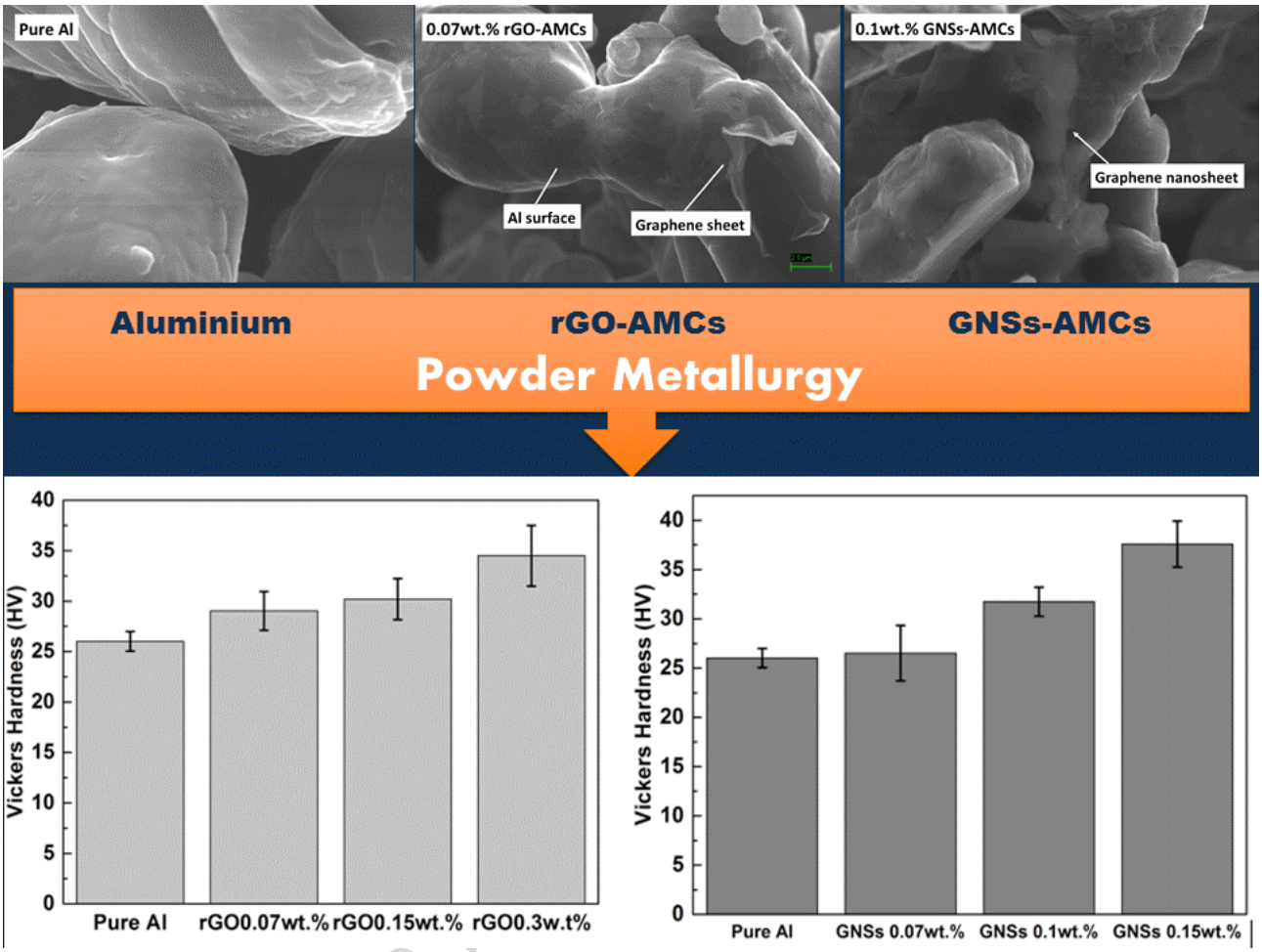

Graphical abstract

Highlights

- Developed powder metallurgy method for rGO and GNS-aluminium matrix composites
- Mechanical and chemical property determination of for graphene-aluminium composites
- Significant increase in composite compact hardness over pure metal baseline
- Correlation of composite density with compaction pressure and reinforcement levels
- Elaboration of areas of focus on method for further improvements in graphene-AMCs